Physica B 406 (2011) 1513–1518

Contents lists available at ScienceDirect

Physica B

journal homepage: www.elsevier.com/locate/physb

Numerical optimization of In-mole fractions and layer thicknesses in $Al_xGa_{1-x}N$/AlN/GaN high electron mobility transistors with InGaN back barriers

O. Kelekci [a,b,*], S.B. Lisesivdin [a], S. Ozcelik [a], E. Ozbay [b,c,d]

[a] Department of Physics, Faculty of Science and Arts, Gazi University, Teknikokullar, 06500 Ankara, Turkey
[b] Nanotechnology Research Center, Bilkent University, Bilkent, 06800 Ankara, Turkey
[c] Department of Physics, Bilkent University, Bilkent, 06800 Ankara, Turkey
[d] Department of Electrical and Electronics Engineering, Bilkent University, Bilkent, 06800 Ankara, Turkey

ARTICLE INFO

Article history:
Received 2 December 2010
Received in revised form
24 January 2011
Accepted 26 January 2011
Available online 1 February 2011

Keywords:
AlGaN/AlN/GaN
HEMT
Schrödinger
Poisson
2DEG
InGaN
Back barrier

ABSTRACT

The effects of the In-mole fraction (x) of an $In_xGa_{1-x}N$ back barrier layer and the thicknesses of different layers in pseudomorphic $Al_yGa_{1-y}N$/AlN/GaN/$In_xGa_{1-x}N$/GaN heterostructures on band structures and carrier densities were investigated with the help of one-dimensional self-consistent solutions of non-linear Schrödinger–Poisson equations. Strain relaxation limits were also calculated for the investigated $Al_yGa_{1-y}N$ barrier layer and $In_xGa_{1-x}N$ back barriers. From an experimental point of view, two different optimized structures are suggested, and the possible effects on carrier density and mobility are discussed.

1. Introduction

The superior material properties of GaN/AlN/InN and the related quaternary and ternary alloys make them the ideal choice for high power and high frequency applications [1,2]. Important progress has been made with improvements in the material quality, device fabrication, and the epitaxial layer designs [3]. However, more advanced device structures are being investigated for further performance improvement. Recently, double-hetero-junction HEMTs were explored to improve carrier confinement, which may result in improved carrier mobility and better pinch-off characteristics for HEMT devices [4–7]. Micovic et al. [4] demonstrated an AlGaN/GaN/AlGaN double-heterojunction HEMT with improved buffer isolation by using an AlGaN buffer layer with an Al composition of 4%. Maeda et al. [5] presented AlGaN/InGaN/AlGaN double heterostructures to improve the confinement of two-dimensional electron gas (2DEG). In addition to all these efforts, thin InGaN layers have also been employed as back

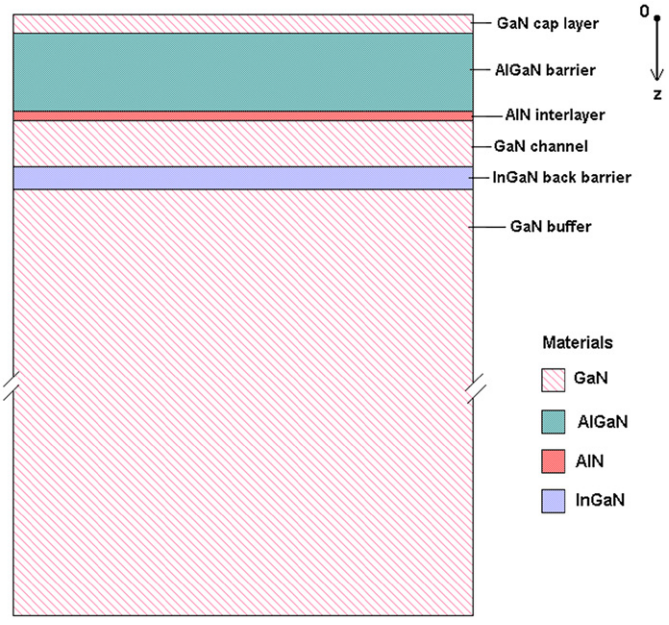

Fig. 1. HEMT structure that was used as a template in the calculations.

* Corresponding author at: Department of Physics, Faculty of Science and Arts, Gazi University, Teknikokullar, 06500 Ankara, Turkey. Tel.: +90312 2903050; fax: +90312 2901015.
E-mail address: okelekci@gmail.com (O. Kelekci).

0921-4526/$ - see front matter © 2011 Elsevier B.V. All rights reserved.
doi:10.1016/j.physb.2011.01.059

barriers (by increasing the conduction band offset of the GaN buffer with respect to the GaN channel) in order to increase the confinement of electrons in the channel [6,7].

GaN-based heterostructures are unique in that the 2DEG is accumulated not by intentional doping, but rather by the polarization charges formed at the interface between the bulk GaN region and the AlGaN barrier layer. These polarization charges are composed of two parts: spontaneous and piezoelectric [8,9]. This property is unlike many other semiconductors and, for this reason, as for the A1GaN/GaN system and other III–V nitrides, the effects of both spontaneous and piezoelectric polarization fields must be included in an electrical analysis. Further investigations and understanding of the energy band diagram and charge distribution, which can be obtained by self-consistent Schrödinger–Poisson calculations, are required for the design and analysis of GaN-based HEMT devices.

In this study, we theoretically investigate the effects of the In-mole fraction (x) of an $In_xGa_{1-x}N$ back barrier layer and the thicknesses of different layers on the carrier densities and band structures in pseudomorphic $Al_yGa_{1-y}N$/AlN/GaN/$In_xGa_{1-x}N$/GaN heterostructures by solving one-dimensional non-linear Schrödinger–Poisson equations self-consistently including polarization induced carriers [10]. The strain relaxation limits were also calculated with a simple critical thickness calculation approach [11].

2. Device structures and simulation

The general layer sequence of the modeled HEMT structures is shown in Fig. 1. All of the layers are assumed to be grown on a GaN buffer pseudomorphically. The optimum values of the

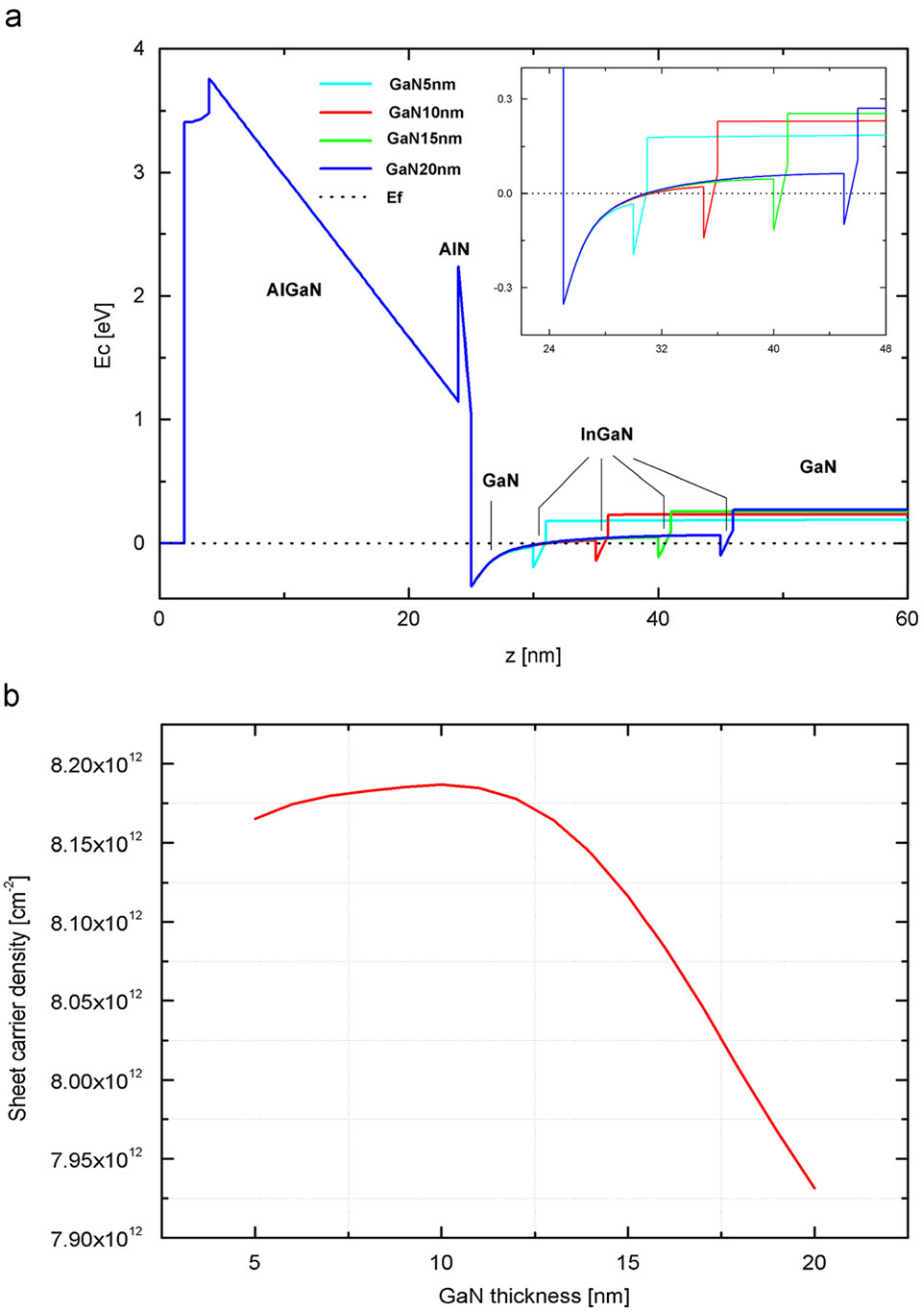

Fig. 2. (a) Calculated conduction band energy diagram of an AlGaN/AlN/GaN/InGaN/GaN HEMT structure with different GaN channel thicknesses. Inset: a closer view of GaN/InGaN region. (b) Sheet carrier density of the designed HEMT structure versus GaN channel thickness.

Al-mole fraction (y) of an $Al_yGa_{1-y}N$ layer, thicknesses of an $Al_yGa_{1-y}N$ layer (t_{AlGaN}), and AlN interlayer (t_{AlN}) for high mobility and carrier concentration in the standard $Al_yGa_{1-y}N$/AlN/GaN HEMTs are well known from the literature [12–14]. Therefore, these values were kept constant throughout the calculations. In the simulations, the In-mole fraction and thickness of the $In_xGa_{1-x}N$ back barrier layer and the thickness of the GaN channel layer are changed systematically, and their effects on the carrier densities and band structures are investigated. The simulation procedure begins with a strain calculation with homogeneous strain dispersion over the simulated region. The strain in a GaN-based material produces a piezoelectric polarization that directly affects the electronic and optical properties of the material. The band edges are calculated by taking account of the van-de-Walle model and strain. With the calculated strain, the piezoelectric charges are then calculated. The quantum states are allocated in previously determined quantum calculation regions. After that, a starting potential value is determined and the non-linear Poisson equation is solved with the calculated piezoelectric and spontaneous charges. In the last step of the simulation, Schrödinger's equation and Poisson's equation are solved self-consistently in order to obtain the carrier distribution, wave functions, and related eigenenergies. The material parameters of AlN, GaN, and InN used in the calculations are taken from several references [15–18]. $In_xGa_{1-x}N$ and $Al_yGa_{1-y}N$ parameters are deduced by using Vegard's law.

The conduction band structures and electron densities are calculated for different layer thicknesses and different In-mole fractions. In every case, the strain values are found to be below the strain relaxation limit for the related structure. A simple estimation for the critical thickness below the strain relaxation limit is given by the relation [11]: $t_{cr} \cong b_e/2\varepsilon_{xx}$. Here, b_e is Burger's vector with a value of $b_e=0.31825$ nm and ε_{xx} is the in-plain strain value for the wurtzite material. A total homogeneous strain over the GaN layer is assumed, which includes the strain values of every layer over the GaN layer.

3. Results and discussion

In order to observe the effects of optimizations, a standard AlGaN/AlN/GaN HEMT structure is first chosen as a template and used for comparison at the end of the optimizations. In this standard structure, $t_{AlGaN}=20$ nm with an Al-mole fraction $y=0.3$ and $t_{AlN}=1$ nm values were used. A higher Al-mole fraction at the barrier layer is required to increase 2DEG conductivity and the breakdown field [19]. However, the growth process of high quality AlGaN layers with high Al content on GaN is problematic due to large lattice mismatch, which can cause defects due to strain relaxation [20]. The critical thickness for $Al_{0.3}Ga_{0.7}N$ is calculated as $t_{critical}=21.8$ nm. First, the GaN channel thickness was changed and the effects of this change on the conduction band and sheet carrier density were analyzed to find an optimum structure. Second, the InGaN back barrier layer's thickness was changed with a constant In-mole fraction. In the last step, the In-mole fraction of the InGaN back barrier layer was scanned with three different thicknesses in order to see the combined effects.

The calculated conduction band energy diagram of an AlGaN/AlN/GaN/InGaN/GaN HEMT structure with different GaN channel thicknesses is shown in Fig. 2a. The sheet carrier density of the designed HEMT structure versus GaN channel thickness is shown in Fig. 2b. In these calculations, the InGaN back barrier layer's thickness is taken as 1 nm, and the In-mole fraction is kept at $x=0.1$. The sheet carrier density increases in very small increments up to 10 nm GaN channel thickness, and makes a peak at this value and starts to decrease more rapidly with thicknesses greater than 12 nm. Although the change in the sheet carrier density is not very significant, the electron confinement effect of the InGaN back barrier layer is smaller for higher GaN channel thicknesses. Therefore, a 10 nm thickness value is chosen as the optimum value for GaN channel thickness.

In Fig. 3, the sheet carrier density of the designed HEMT structure is shown for different InGaN back barrier thicknesses. In these calculations, the InGaN back barrier layer thickness is swept from 1 to 6 nm, and the In-mole fraction is kept at $x=0.1$. The critical thickness of $In_{0.1}Ga_{0.9}N$ on GaN is calculated as 14.4 nm and, therefore, the InGaN layer used here is assumed to be strained. The GaN channel thickness is taken as 10 nm, which is found to be an optimal value in the previous step. There is no considerable change in sheet carrier density with respect to the InGaN back barrier thickness after 3 nm value. It is known that the potential barrier, formed by the InGaN layer, increases with the increase in the InGaN layer thickness [21]. However, as the InGaN layer thickness increases the conduction band offset at the interface between the InGaN-notch and GaN buffer loses its sharpness. As a result, the degree of electron confinement and, therefore, electron mobility is expected to decrease. For the next step of the simulations, the InGaN layer thickness is changed from 1 to 3 nm because more variations are observed and the maximum level is obtained in this interval.

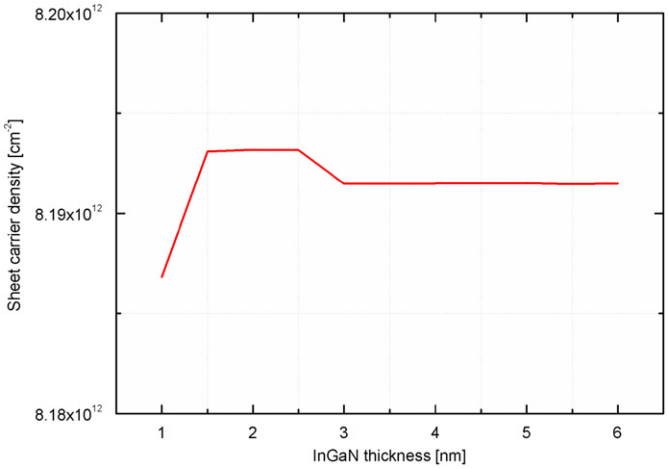

Fig. 3. Sheet carrier density of the designed HEMT structure versus the InGaN back barrier thickness.

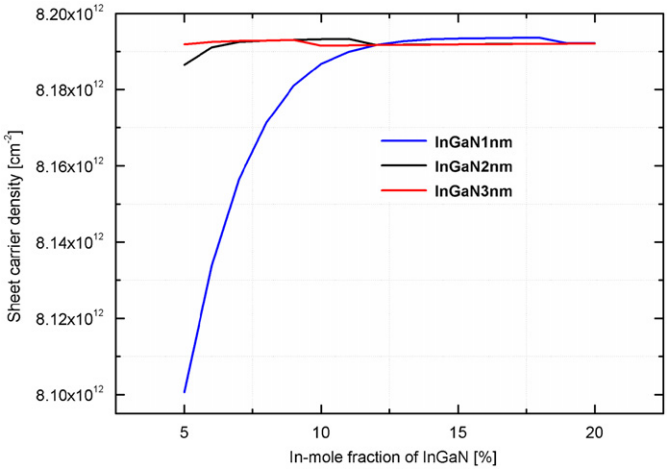

Fig. 4. Sheet carrier density of the designed HEMT structure versus the In-mole fraction of the InGaN back barrier.

Fig. 4 shows the sheet carrier density of the designed HEMT structure versus the In-mole fraction values of the InGaN back barrier layer with different thicknesses. In these calculations, the In-mole fraction is swept from 5% to 20%, and InGaN layer thickness is varied from 1 to 3 nm. As can be seen in the figure, the sheet carrier density is much more dependent on the In-mole fraction for 1 nm thickness when compared to 2 and 3 nm thicknesses. The maximum sheet carrier density is obtained for a 1 nm thick $In_{0.18}Ga_{0.82}N$ layer. Another option for the back barrier would be a 3 nm thick $In_{0.09}Ga_{0.91}N$ layer because the sheet carrier density obtained with this layer is very close to that of a 1 nm thick $In_{0.18}Ga_{0.82}N$ layer. Therefore, one has to carry out further analysis for these two different configurations.

Conduction band diagrams for the structures with 1 and 3 nm thick InGaN layers with varying In-mole fractions are shown in Figs. 5a and b, respectively. In Fig. 5c, the carrier density distributions for 1 nm and 3 thick InGaN back barriers are compared. The InGaN channel is more populated for the structure with 1 nm thick $In_{0.18}Ga_{0.82}N$ when compared to 3 nm thick $In_{0.09}Ga_{0.91}N$. This can be seen as a disadvantage but from the figure it is possible to conclude that these electrons are well confined and spillover to the major channel will not occur. It is also clearly seen that electrons are more likely to spread into the GaN buffer layer for the structure with 3 nm thick InGaN back barrier. Therefore, we proposed an optimum $Al_{0.3}Ga_{0.7}N/AlN/GaN/In_{0.18}Ga_{0.82}N/GaN$ HEMT structure for high 2DEG concentration and mobility with thicknesses of 20, 1, 10, and 1 nm for the layers $Al_{0.3}Ga_{0.7}N$, AlN, GaN, and $In_{0.18}Ga_{0.82}N$, respectively. However, it should be noted that sheet carrier density dependency to the In-mole fraction for this structure is an important issue from an experimental point of view because it is difficult to precisely control the In-mole fraction of the InGaN layer in growth processes [22]. The calculated conduction band energy diagrams of standard AlGaN/AlN/GaN structure and an optimized structure with an InGaN back barrier is shown in Fig. 6a. In Fig. 6b, carrier density distributions for standard AlGaN/AlN/GaN structure and an optimized structure with an InGaN back barrier are compared. According to the calculation results, a 16.6% increase in the sheet carrier density can be expected by using an InGaN back barrier and by optimizing the layers properly.

4. Conclusions

We have modeled $Al_yGa_{1-y}N/AlN/GaN/In_xGa_{1-x}N/GaN$ HEMT structures by solving one-dimensional non-linear Schrödinger–Poisson equations self-consistently. Conduction band diagrams

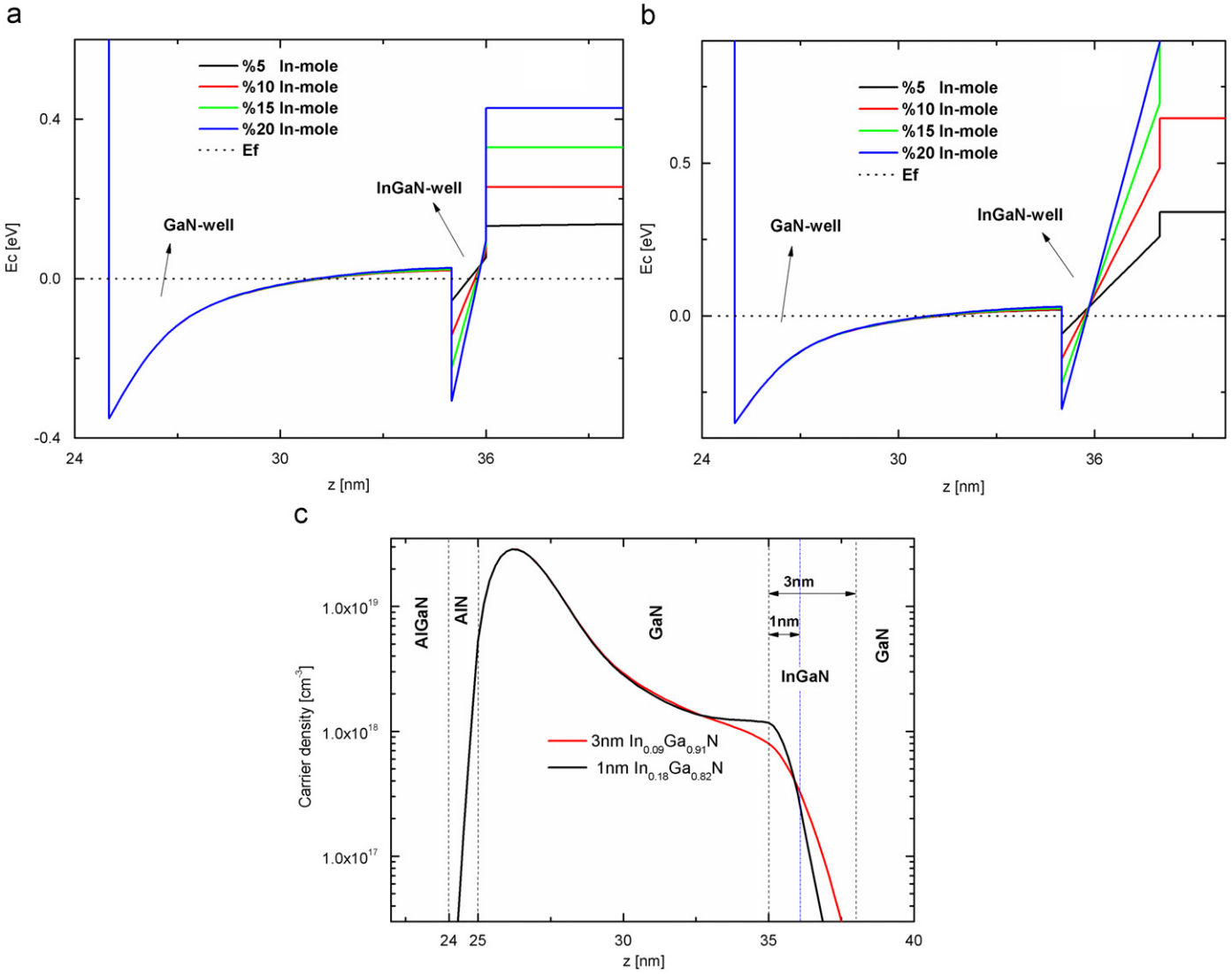

Fig. 5. (a) Calculated conduction band energy diagrams of the designed HEMT structures with 1 nm and (b) 3 nm thick InGaN back barriers. (c) Comparison of carrier density distributions for 1 and 3 nm thick InGaN back barriers.

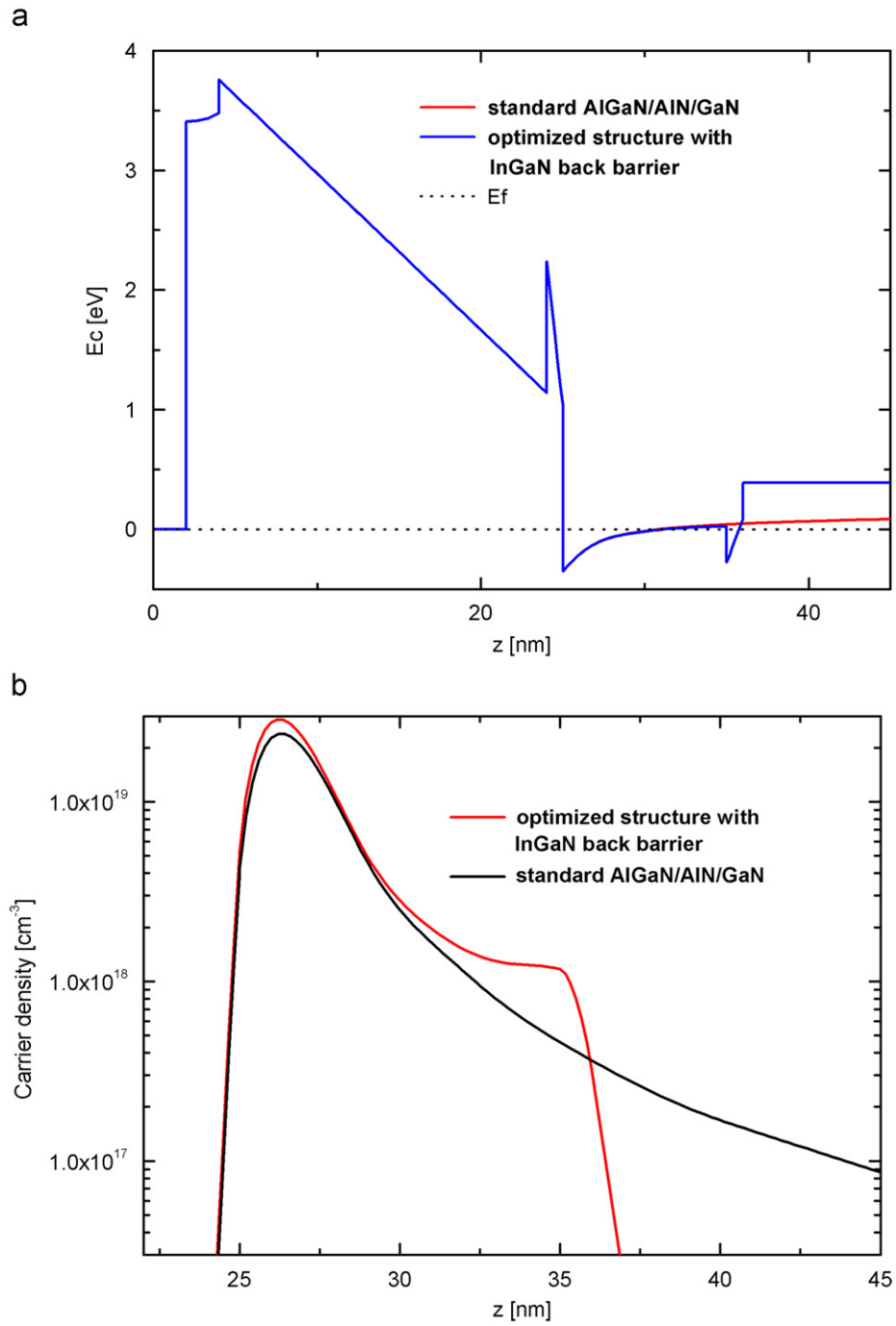

Fig. 6. (a) Calculated conduction band energy diagrams of a standard AlGaN/AlN/GaN structure and optimized structure with an InGaN back barrier (b) Comparison of the carrier density distributions for a standard AlGaN/AlN/GaN structure and optimized structure with an InGaN back barrier.

and sheet carrier densities are calculated for different GaN channel and $In_xGa_{1-x}N$ back barrier layer thicknesses and for different In-mole fractions, including piezoelectric and spontaneous polarization fields. The effects of the GaN channel thickness, InGaN back barrier thickness, and In-mole fraction were investigated in order to increase carrier density and mobility. The pseudomorphic conditions were also satisfied for all the simulations, in which the optimizations were limited within the strain relaxation limits. According to the optimization results, $Al_{0.3}Ga_{0.7}N/AlN/GaN/In_{0.18}Ga_{0.82}N/GaN$ structure with a thickness sequence of 20/1/10/1 nm is proposed for the high-performance devices with a high mobility and high carrier density. From an experimental point of view, $Al_{0.3}Ga_{0.7}N/AlN/GaN/In_{0.09}Ga_{0.91}N/GaN$ structure with a thickness sequence of 20/1/10/3 nm should also be taken into account. According to the calculations, a 16.6% increase in sheet carrier density is predicted for an optimized AlGaN/AlN/GaN/InGaN/GaN structure compared to conventional AlGaN/AlN/GaN HEMT structures.

These simulation results show that, if optimized properly, AlGaN/AlN/GaN/InGaN/GaN heterostructures have the potential to be a promising structure for making high-performance GaN-based HEMTs due to their superior channel confinement and 2DEG density.

Acknowledgments

This work is supported by the State Planning Organization of Turkey under Grant No. 2001K120590 by the European Union under the projects EU-PHOME and EU-ECONAM, and TUBITAK under the Project nos. 106E198, 107A004, and 107A012. One of the authors (Ekmel Ozbay) acknowledges partial support from the Turkish Academy of Sciences.

References

[1] M.S. Shur, Solid State Electron. 42 (1998) 2131.
[2] H. Morkoç, Handbook of Nitride Semiconductors and Devices, vol. 3, Wiley-VCH Verlag GmbH, 2009.
[3] U.K. Mishra, L. Shen, T.E. Kazior, Y.-F. Wu, Proc. IEEE 96 (2008) 287.
[4] M. Micovic, P. Hashimoto, Hu Ming, I. Milosavljevic, J. Duvall, P.J. Willadsen, W.-S. Wong, A.M. Conway, A. Kurdoghlian, P.W. Deelman, M. Jeong-S, A. Schmitz, M.J. Delaney, IEDM Technical Digest, 2004, pp. 807–810.
[5] N. Maeda, T. Saitoh, K. Tsubaki, T. Nishida, N. Kobayashi, Jpn. J. Appl. Phys. 38 (1999) L799.
[6] J. Liu, Y. Zhou, J. Zhu, K.M. Lau, K.J. Chen, IEEE Electron. Device Lett. 27 (2006) 10.
[7] T. Palacios, A. Chakraborty, S. Heikman, S. Keller, S.P. DenBaars, U.K. Mishra, IEEE Electron. Device Lett. 27 (2006) 13.
[8] A. Bykhovski, B. Gelmont, M. Shur, J. Appl. Phys. 74 (1993) 6734.
[9] F. Bernardini, V. Fiorentini, Phys. Rev. B 56 (1997) 10024.
[10] S. Birner, S. Hackenbuchner, M. Sabathil, G. Zandler, J.A. Majewski, T. Andlauer, T. Zibold, R. Morschl, A. Trellakis, P. Vogl, Acta Phys. Pol. A 110 (2006) 111.
[11] J. Singh, Physics of Semiconductors and Their Heterostructures, McGraw-Hill, New York, 1992, p. 734.
[12] I.P. Smorchkova, L. Chen, T. Mates, L. Shen, S. Heikman, B. Moran, S. Keller, S.P. DenBaars, J.S. Speck, U.K. Mishra, J. Appl. Phys. 90 (2001) 5196.
[13] Z. Bougrioua, J.-L. Farvacque, I. Moerman, F. Carosella, Phys. Status Solidi (b) 228 (2) (2001) 625–628.
[14] S.B. Lisesivdin, A. Yildiz, M. Kasap, Optoelectron. Adv. Mater. - Rapid Comm. 1 (2007) 467.
[15] I. Vurgaftman, J.R. Meyer, L.R. Ram-Mohan, J. Appl. Phys. 89 (2001) 5815.
[16] I. Vurgaftman, J.R. Meyer, J. Appl. Phys. 94 (2003) 3675.
[17] O. Ambacher, J. Majewski, C. Miskys, A. Link, M. Hermann, M. Eickhoff, M. Stutzmann, F. Bernardini, V. Fiorentini, V. Tilak, B. Schaff, L.F. Eastman, J. Phys. Condens. Matter 14 (2002) 3399.
[18] H. Morkoç, Nitride Semiconductors and Devices, Springer-Verlag, Berlin Heidelberg, 1999.
[19] Y.–F. Wu, D. Kapolnek, J.P. Ibbetson, P. Parikh, B.P. Keller, U.K. Mishra, T. IEEE, Electron. Dev. 48 (2001) 586.
[20] B. Shen, T. Someya, Y. Arakawa, Appl. Phys. Lett. 76 (2000) 2746.
[21] J. Tang, X. Wang, H. Xiao, J. Ran, C. Wang, X. Wang, G. Hu, J. Li, Phys. Status Solidi (c) 5 (2008) 2982.
[22] J. Liberis, I. Matulionienė, A. Matulionis, E. Šermukšnis, J. Xie, J.H. Leach, H. Morkoç, Phys. Status Solidi (a) 206 (2009) 1385.